DOI: 10.1002/ejic.201001058

Magnetic Properties of [FeFe]-Hydrogenases: A Theoretical Investigation Based on Extended QM and QM/MM Models of the H-Cluster and Its Surroundings

Claudio Greco,*[a] Alexey Silakov,*[b] Maurizio Bruschi,[c] Ulf Ryde,[d] Luca De Gioia,[a] and Wolfgang Lubitz[b]

Keywords: Computer chemistry / Density functional calculations / Magnetic properties / EPR parameters calculation / Quantum mechanics / Enzymes / Hydrogenases / Hydrogen

In the present contribution, we report a theoretical investigation of the magnetic properties of the dihydrogen-evolving enzyme [FeFe]-hydrogenase, based on both DFT models of the active site (the H-cluster, a Fe_6S_6 assembly including a binuclear portion directly involved in substrates binding), and QM/MM models of the whole enzyme. Antiferromagnetic coupling within the H-cluster has been treated using the broken-symmetry approach, along with the use of different density functionals. Results of *g* value calculations turned out to vary as a function of the level of theory and of the extension of the model. The choice of the broken-symmetry coupling scheme also had a significant influence on the calculated *g* values, for both the active-ready (H_{ox}) and the CO-inhibited (H_{ox}-CO) enzyme forms. However, hyperfine coupling-constant calculations were found to provide more consistent results. This allowed us to show that the experimentally detected delocalization of an unpaired electron at the binuclear subcluster in *Desulfovibrio desulfuricans* H_{ox} is compatible with a weak interaction between the catalytic centre and a low-weight exogenous ligand like a water molecule.

Introduction

[FeFe]-hydrogenases are dihydrogen-evolving/oxidising enzymes that possess a peculiar Fe_6S_6 complex in their active site (the "H-cluster", see Figure 1). The key steps underlying catalysis take place at a specific binuclear portion of the H-cluster. This binuclear subcluster, generally referred to as $[2Fe]_H$, is linked to the remaining tetranuclear portion of the active site (which will be referred to as the $[4Fe\text{-}4S]_H$ subcluster) by means of a cysteine sulfur atom (S_1 in Figure 1).

The disclosure of the H-cluster structural features by means of X-ray crystallography has allowed researchers to investigate the enzyme structure in detail.[1–4] In this context, spectroscopic investigations based on IR absorption

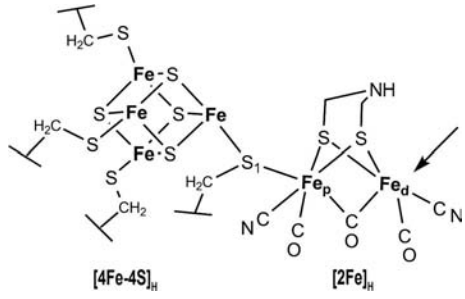

Figure 1. Schematic representation of the H-cluster.

deepened our insights of the peculiar coordination environment of metal centres in the $[2Fe]_H$ subcluster:[5–7] the latter features the biologically unusual presence of cyanide and carbonyl ligands. One of the CO groups turned out to be in bridging position between the two iron atoms in all the enzymatic states, except for the completely reduced enzyme, in which it moves to a terminal position.[4,7] The H-cluster can attain different redox states: the partially oxidised, CO-bridged form features a paramagnetic, mixed valence $Fe^{I}Fe^{II}$ redox state at the $[2Fe]_H$ subsite,[8,9] while the $[4Fe\text{-}4S]_H$ subcluster attains the $2Fe^{II}2Fe^{III}$ state.[9,10] This form of the H-cluster, usually referred to as "H_{ox}", is thought to be able to bind exogenous H_2 at the vacant coordination site indicated by an arrow in Figure 1 (this iron ion is termed "distal", Fe_d, while the second metal ion in the subcluster is termed "proximal", Fe_p, based on their relative

[a] Department of Biotechnology and Biosciences, University of Milan-Bicocca,
Piazza della Scienza 2, 20126 Milan, Italy
Fax: +39-02-64483478
E-mail: claudio.greco@unimib.it
[b] Max Planck Institute for Bioinorganic Chemistry,
Stiftstrasse 34–36, 45468 Mülheim/Ruhr, Germany
Fax: +49-208-3063951
E-mail: silakov@mpi-muelheim.mpg.de
[c] Department of Environmental Sciences, University of Milan-Bicocca,
Piazza della Scienza 1, 20126 Milan, Italy
[d] Department of Theoretical Chemistry, Lund University,
Chemical Center,
P. O. B. 124, 22100 Lund, Sweden
Supporting information for this article is available on the WWW under http://dx.doi.org/10.1002/ejic.201001058.

positions with respect to the tetranuclear portion of the H-cluster).[4,11,12] Notably, the Fe_d center in H_{ox} can also bind exogenous CO, giving rise to the CO-inhibited form of the enzyme, H_{ox}-CO.[3,6,13,14] Single-electron reduction of H_{ox} yields the reduced, H_{red} form of the active site, which is able to bind protons, thus starting the catalytic process of H_2 evolution.[9,12,15] H_{red} is a diamagnetic state of the H-cluster, characterized by the $Fe^{I}Fe^{I}$ and $2Fe^{II}2Fe^{III}$ states of the $[2Fe]_H$ and $[4Fe\text{-}4S]_H$ subclusters, respectively.[9]

In this paper, which is focussed on the magnetic properties of the H-cluster, we present for the first time theoretical results on the EPR parameters and hyperfine couplings of the entire H-cluster in the paramagnetic forms H_{ox} and H_{ox}-CO. The models are geometry-optimized using density functional theory (DFT), and the environment of the H-cluster is represented by using either a continuum solvent model (COSMO)[16] or by means of an explicit all-atom representation of the protein matrix based on molecular mechanics (MM). The results are compared with those obtained using simple Fe_2S_2 models of the isolated $[2Fe]_H$ subcluster.[14,17–19]

As noted in previous studies, reproduction of the experimental EPR *g* factors and hyperfine couplings of hydrogenases is a challenging task;[14,17–20] in particular, previous theoretical studies based on simple models of the $[2Fe]_H$ subsite gave only partially satisfactory results for the H_{ox} and H_{ox}-CO states.[14,17–19] This might be due to one or more of the following reasons: (i) models of the isolated $[2Fe]_H$ subcluster completely neglect the electronic effects of the $[4Fe\text{-}4S]_H$ subcluster, which are thought to play a relevant role in the [FeFe]-hydrogenase chemistry;[15,21,22] (ii) a poor reproduction of the environment of the H-cluster might prevent the fine reproduction of the geometrical and electronic features of the latter, thus affecting the quality of the magnetic properties calculations;[18,21] (iii) from a methodological point of view, the accuracy of electron densities obtained by DFT methods is also a matter of concern for the calculation of magnetic properties; (iv) finally, the possible presence of labile ligands such as metal-bound water molecules might deeply affect the H-cluster electron density, a point that has not been thoroughly investigated. The above issues have been tackled in this paper, by performing magnetic properties computation at different levels of theory and by including in the models the effects of the $[4Fe\text{-}4S]_H$ subsite and of the surrounding protein matrix. The antiferromagnetic coupling characterizing the $[4Fe\text{-}4S]_H$ subcluster was treated using the broken-symmetry (BS) approach,[23] which is based on localizing opposite spins on selected Fe_2S_2 layers composing the tetranuclear H-cluster subsite.[15,19] The possibility that a water ligand might be bound to the distal iron atom in H_{ox} was also taken into account.

Results and Discussion

1. H_{ox}-CO Models

The calculated hyperfine couplings and *g* factors for the H_{ox}-CO form of the enzyme are reported in Table 1. Let us first analyze the isolated, Fe_6S_6 models optimized in the COSMO continuum solvent. Two models were considered: **1-$Fe_6S_6^{BS1}$** and model **1-$Fe_6S_6^{BS2}$**, Figure 2. These models differ in terms of broken-symmetry coupling scheme as described in Methods. A comparison between the experimental *g* factors of *Desulfovibrio desulfuricans* hydrogenase (DdH) (g_1 = 2.00; g_2 = 2.01; g_3 = 2.07)[21] and theoretical B3LYP results for **1-$Fe_6S_6^{BS1}$** (g_1 = 1.98, g_2 = 2.02, g_3 = 2.06) would indicate that *g* values can be accurately reproduced. However, it must be pointed out that the BS1 state is higher in energy than the alternative BS2 state (ΔE = 12 kJ/mol), and switching to the latter wavefunction leads to a quite large change in the computed g_2 and g_3 values, so that g_3 becomes as low as 2.03, while g_2 is now smaller by 0.02. This illustrates how the choice of BS solutions is non-innocent in terms of *g* factors calculations.

Table 1. *g* factors, hyperfine couplings and Mulliken populations calculated at the B3LYP/TZVP level on H_{ox}-CO models **1**. Experimental data are also included.[21]

Model name	*g* factors	Hyperfine couplings [MHz]	Mulliken spin population
1-$Fe_6S_6^{BS1}$	g_1 = 1.98	Fe_p = 22.9	Fe_p = 0.45
	g_2 = 2.02	Fe_d = 13.0	Fe_d = 0.37
	g_3 = 2.06	C_{exg} = 51.9	
1-$Fe_6S_6^{BS2}$	g_1 = 1.98	Fe_p = 22.0	Fe_p = 0.47
	g_2 = 2.00	Fe_d = 11.9	Fe_d = 0.35
	g_3 = 2.03	C_{exg} = 49.3	
1-$Fe_2S_2^{TRUNC}$	g_1 = 2.01	Fe_p = 29.1	Fe_p = 0.59
	g_2 = 2.02	Fe_d = 10.0	Fe_d = 0.29
	g_3 = 2.03	C_{exg} = 38.2	
1-Fe_2S_2_surr	g_1 = 2.01	Fe_p = 25.1	Fe_p = 0.53
	g_2 = 2.01	Fe_d = 11.3	Fe_d = 0.33
	g_3 = 2.02	C_{exg} = 38.2	
1-$DdH^{QM/MM}$	g_1 = 1.99	Fe_p = 22.5	Fe_p = 0.50
	g_2 = 2.01	Fe_d = 12.1	Fe_d = 0.36
	g_3 = 2.05	C_{exg} = 54.3	
Exp.	g_1 = 2.00	Fe_p = 4.0	–
	g_2 = 2.01	Fe_d = 0.8	–
	g_3 = 2.07	C_{exg} = 17.1	–

Removing the Fe_4S_4 cluster from the model (**1-$Fe_2S_2^{TRUNC}$**, obtained by truncation of **1-$Fe_6S_6^{BS1}$**) leads to a quite large change in the computed *g* values (g_1 = 2.01, g_2 = 2.02, g_3 = 2.03). Now, the two theoretical *g* values that better reproduce the corresponding experimental values are g_1 and g_2. In fact, the difference between theory and experiment for g_3 is as large as 0.04; notice also that the *g* factors calculated for **1-$Fe_2S_2^{TRUNC}$** are essentially indistinguishable from those previously obtained by Brunold et al. on Fe_2S_2 models truncated by the inclusion of a $SHCH_3$ moiety and studied using the BP86 functional and the zeroth-order regular approximation (ZORA) Hamiltonian (in that case, the *g* values calculated with ORCA were the following: g_1 = 2.01, g_2 = 2.02, g_3 = 2.03).[19] The inclusion in the QM model of the protein portion in the immediate neighborhood of the $[2Fe]_H$ cluster (**1-Fe_2S_2_surr**) leads to a picture close to the one already described for **1-$Fe_2S_2^{TRUNC}$** (see Table 1). On the contrary, optimization of the H-cluster in an all-atom representation of the whole DdH enzyme

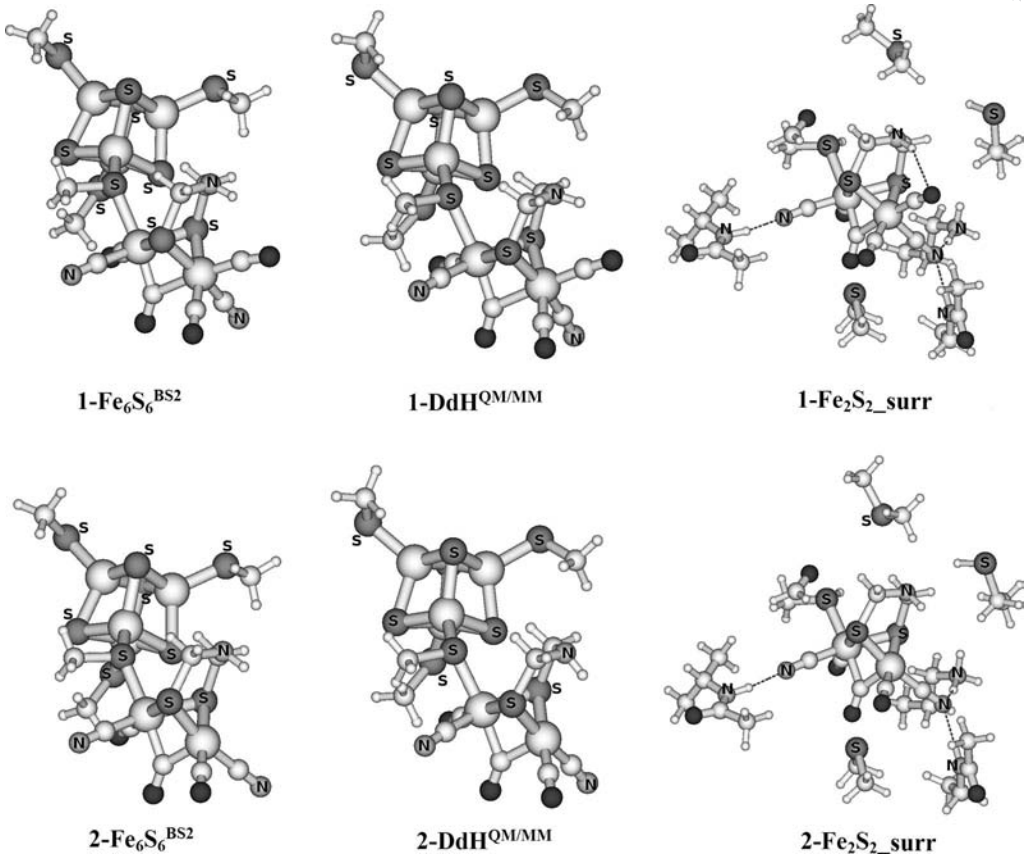

Figure 2. Upper row: geometries of models **1-Fe$_6$S$_6^{BS2}$**, **1-DdH$^{QM/MM}$** and **1-Fe$_2$S$_2$_surr**. Notice that the CH_3SH fragment representing Cys178 (see chapter Methods), which belongs to the QM region of both the QM/MM models **1-DdH$^{QM/MM}$** and **2-DdH$^{QM/MM}$**, has been omitted in the present pictorial representation, for the sake of clarity. Small, middle-size and large white spheres correspond to hydrogen, carbon and iron atoms, respectively; dark grey, middle-size spheres represent oxygen atoms. Lower row: geometries of models **2-Fe$_6$S$_6^{BS2}$**, **2-DdH$^{QM/MM}$** and **2-Fe$_2$S$_2$_surr**.

(model **1-DdH$^{QM/MM}$**, see chapter Methods below) leads to computed *g* factors that are closer to experiment: $g_1 = 1.99$, $g_2 = 2.01$, $g_3 = 2.05$. The maximum difference between these *g* factors and experimental data is 0.02 (for g_3).

As for the choice of the density functional for H-cluster *g* factors calculations, B3LYP results are generally closer to experimental results, while BP86 results are more similar to each other when different models are taken into account (see Tables 1 and 2).

Finally, hyperfine couplings of the Fe_p and Fe_d centres and of the carbon atom of the Fe_d-bound exogenous CO group have also been computed. It turned out that they are generally overestimated (see Table 1, where the corresponding experimental values for DdH are also reported).[21] For example, while the experimental hyperfine couplings in DdH turned out to be 4.0 and 0.8 MHz for the Fe_p and Fe_d centres, respectively, the corresponding computed values for the enzyme model **1-DdH$^{QM/MM}$** are as large as 22.5 and 12.1 MHz in the case of B3LYP models. In other words, the theoretical couplings of Fe_p and Fe_d are approximately 5–12 times larger that the corresponding experimental data, indicating that the spin excess on the metal centres is overestimated in the model. Very similar conclusions can be drawn for the C atom of the exogenous carbonyl ligand (the calculated value for **1-DdH$^{QM/MM}$** was 54.3 MHz, compared to the experimental value of 17.1 MHz). Notably, an

Table 2. *g* factors, hyperfine couplings and Mulliken populations calculated at the BP86/TZVP level on H_{ox}-CO models **1**. Experimental data are also included.[21]

Model name	*g* factors	Hyperfine couplings [MHz]	Mulliken spin population
1-Fe$_6$S$_6^{BS1}$	$g_1 = 1.97$	$Fe_p = 20.7$	$Fe_p = 0.50$
	$g_2 = 2.02$	$Fe_d = 7.6$	$Fe_d = 0.27$
	$g_3 = 2.02$	$C_{exg} = 67.5$	
1-Fe$_6$S$_6^{BS2}$	$g_1 = 1.99$	$Fe_p = 18.1$	$Fe_p = 0.43$
	$g_2 = 2.01$	$Fe_d = 6.3$	$Fe_d = 0.23$
	$g_3 = 2.04$	$C_{exg} = 58.6$	
1-Fe$_2$S$_2^{TRUNC}$	$g_1 = 2.00$	$Fe_p = 26.9$	$Fe_p = 0.58$
	$g_2 = 2.01$	$Fe_d = 6.4$	$Fe_d = 0.23$
	$g_3 = 2.02$	$C_{exg} = 56.1$	
1-Fe$_2$S$_2$_surr	$g_1 = 2.00$	$Fe_p = 22.9$	$Fe_p = 0.54$
	$g_2 = 2.01$	$Fe_d = 7.1$	$Fe_d = 0.26$
	$g_3 = 2.02$	$C_{exg} = 63.9$	
1-DdH$^{QM/MM}$	$g_1 = 1.99$	$Fe_p = 20.4$	$Fe_p = 0.51$
	$g_2 = 2.01$	$Fe_d = 6.9$	$Fe_d = 0.26$
	$g_3 = 2.02$	$C_{exg} = 67.5$	
Exp.	$g_1 = 2.00$	$Fe_p = 4.0$	–
	$g_2 = 2.01$	$Fe_d = 0.8$	–
	$g_3 = 2.07$	$C_{exg} = 17.1$	–

analogous hyperfine coupling was previously obtained by B3LYP computations on binuclear H-cluster models truncated by a CH_3S^- fragment.[19] Overestimation of the hyperfine couplings was observed also for the BP86 results (Table 2). However, in this case the ratio between experimental couplings for Fe_p and Fe_d in DdH (4.0/0.8 = 5) is in reasonable agreement with theory (ratio around 3 and 4.2 for **1-DdH$^{QM/MM}$** and **1-Fe$_2$S$_2^{TRUNC}$**, respectively; see Table 2). As for the ratio between the hyperfine couplings of the Fe_p centre and the C atom of the exogenous CO ligand, the experimental and computational values are again not too far from each other (experimental ratio: 0.23; calculated ratios: 0.30 and 0.48 for models **DdH$^{QM/MM}$** and **1-Fe$_2$S$_2^{TRUNC}$**, respectively; Table 2). Notice that the computed couplings do not vary appreciably when going from the binuclear to the hexanuclear models, because the extension of the QM representation to the entire H-cluster does not cause any redistribution of spin over the atoms composing the model (see spin population of the Fe_p and Fe_d centres in Tables 1 and 2).

2. H_{ox} Models

Let us now analyze the H_{ox} state of the enzyme. We have first investigated models showing a vacant coordination site on Fe_d (see models of the **2** type in Figure 2). The COSMO-optimized Fe_6S_6 model of the isolated H-cluster **2-Fe$_6$S$_6^{BS1}$** gives $g_1 = 2.03$, $g_2 = 2.06$, $g_3 = 2.10$ (Table 3, B3LYP results). These computed EPR parameters qualitatively reproduce the general features of the experimental spectrum for the partially oxidized DdH enzyme: $g_1 = 2.00$, $g_2 = 2.04$, $g_3 = 2.10$. However, a quite different g_1 value (1.97) is obtained when considering the **2-Fe$_6$S$_6^{BS2}$** model, where the spin density pattern at the $[4Fe\text{-}4S]_H$ subcluster is changed. Note also that **2-Fe$_6$S$_6^{BS2}$** shows a very small energy difference relative to **2-Fe$_6$S$_6^{BS1}$** ($\Delta E_{BS1-BS2}$ = 3 kJ/mol). In this context, it is worth noting that an average set of g values obtained from the two BS states ($g_1 = 2.00$, $g_2 = 2.06$, $g_3 = 2.10$) is closer to the experimental results, compared to the g values of the models considered separately. Such average set of g factors is also similar to the g values calculated for the truncated Fe_2S_2 model **2-Fe$_2$S$_2^{TRUNC}$** ($g_1 = 2.01$, $g_2 = 2.05$, $g_3 = 2.09$). The extended **2-Fe$_2$S$_2$_surr** model gives theoretical g factors similar to those of the naked Fe_2S_2 model ($g_1 = 2.01$, $g_2 = 2.06$, $g_3 = 2.09$, Table 3). On the other hand, the QM/MM model **2-DdH$^{QM/MM}$** gives computed g factors rather far from the experimental values ($g_1 = 2.04$, $g_2 = 2.07$, $g_3 = 2.09$). However, truncation of the QM/MM optimized H-cluster to a $[2Fe]_H$ model gives g factors ($g_1 = 2.01$, $g_2 = 2.05$, $g_3 = 2.09$), that are the same as those computed for **2-Fe$_2$S$_2^{TRUNC}$**. The computed g values for the truncated models are close to the theoretical values reported by Brunold et al. ($g_1 = 2.012$, $g_2 = 2.035$, $g_3 = 2.085$).[19] Finally, the BP86 method reproduces the experimental g_1 value better than B3LYP, but the opposite is found for g_3 (see Table 4).

Table 3. g factors, hyperfine couplings and Mulliken populations calculated at the B3LYP/TZVP level on H_{ox} models **2**. Experimental data are also included.[21]

Model name	g factors	Hyperfine couplings [MHz]	Mulliken spin population
2-Fe$_6$S$_6^{BS1}$	$g_1 = 2.03$	$Fe_p = 2.0$	$Fe_p = 0.13$
	$g_2 = 2.06$	$Fe_d = 32.9$	$Fe_d = 1.07$
	$g_3 = 2.10$		
2-Fe$_6$S$_6^{BS2}$	$g_1 = 1.97$	$Fe_p = 0.1$	$Fe_p = 0.10$
	$g_2 = 2.05$	$Fe_d = 32.6$	$Fe_d = 1.04$
	$g_3 = 2.09$		
2-Fe$_2$S$_2^{TRUNC}$	$g_1 = 2.01$	$Fe_p = 0.4$	$Fe_p = 0.10$
	$g_2 = 2.05$	$Fe_d = 31.8$	$Fe_d = 1.05$
	$g_3 = 2.09$		
2-Fe$_2$S$_2$_surr	$g_1 = 2.01$	$Fe_p = 2.3$	$Fe_p = 0.14$
	$g_2 = 2.06$	$Fe_d = 31.8$	$Fe_d = 0.96$
	$g_3 = 2.09$		
2-DdH$^{QM/MM}$	$g_1 = 2.04$	$Fe_p = 3.1$	$Fe_p = 0.15$
	$g_2 = 2.07$	$Fe_d = 34.9$	$Fe_d = 1.14$
	$g_3 = 2.09$		
Exp.	$g_1 = 2.00$	$Fe_p = 12.4$	–
	$g_2 = 2.04$	$Fe_d = 12.4$	–
	$g_3 = 2.10$		

Table 4. g factors, hyperfine couplings and Mulliken populations calculated at the BP86/TZVP level on H_{ox} models **2**. Experimental data are also included.[21]

Model name	g factors	Hyperfine couplings [MHz]	Mulliken spin population
2-Fe$_6$S$_6^{BS1}$	$g_1 = 2.00$	$Fe_p = 2.9$	$Fe_p = 0.18$
	$g_2 = 2.03$	$Fe_d = 25.3$	$Fe_d = 0.91$
	$g_3 = 2.07$		
2-Fe$_6$S$_6^{BS2}$	$g_1 = 2.00$	$Fe_p = 0.6$	$Fe_p = 0.14$
	$g_2 = 2.04$	$Fe_d = 24.3$	$Fe_d = 0.86$
	$g_3 = 2.07$		
2-Fe$_2$S$_2^{TRUNC}$	$g_1 = 2.01$	$Fe_p = 1.2$	$Fe_p = 0.14$
	$g_2 = 2.03$	$Fe_d = 25.0$	$Fe_d = 0.91$
	$g_3 = 2.06$		
2-Fe$_2$S$_2$_surr	$g_1 = 2.01$	$Fe_p = 2.5$	$Fe_p = 0.17$
	$g_2 = 2.04$	$Fe_d = 27.4$	$Fe_d = 0.84$
	$g_3 = 2.06$		
2-DdH$^{QM/MM}$	$g_1 = 2.01$	$Fe_p = 3.8$	$Fe_p = 0.16$
	$g_2 = 2.04$	$Fe_d = 27.5$	$Fe_d = 0.88$
	$g_3 = 2.07$		
Exp.	$g_1 = 2.00$	$Fe_p = 12.4$	–
	$g_2 = 2.04$	$Fe_d = 12.4$	–
	$g_3 = 2.10$		

For the hyperfine couplings, it is worth noting that identical hyperfine couplings were experimentally measured for the proximal and the distal iron, while in the calculations the couplings differ by about one order of magnitude. In particular, calculated Fe_p couplings turned out to be too low in all models, while the opposite is true for Fe_d. This applies to both B3LYP (Table 3) and BP86 (Table 4) results.

3. H_{ox}-H_2O Models

Finally, we consider H_{ox} models with a water molecule bound to the Fe_d centre (model of the **3** type, see Figure S2 in the Supporting Information). In this case, all the investi-

gated Fe_2S_2 and Fe_6S_6 models give *g* factors that do not fit so accurately the experimental data, with deviations equal to or larger than 0.03 for one or more of the *g* factors (B3LYP results, see Table 5). In particular, in specific models such as the constrained Fe_6S_6 models, the BS2 state, which is lower in energy than the BS1 model ($\Delta E_{BS1-BS2}$ = 23 kJ/mol), *g* values (g_1 = 1.97, g_2 = 2.03, g_3 = 2.06, Table 5) are quite far from corresponding experimental values. The BP86 functional also fails to fully satisfactorily reproduce the experimental *g* values (see Table 6).

Table 5. *g* factors, hyperfine couplings and Mulliken populations calculated at the B3LYP/TZVP level on H_{ox} models **3**. Experimental data are also included.[21]

Model name	*g* factors	Hyperfine couplings [MHz]	Mulliken spin population
3-$Fe_6S_6^{BS1}$	g_1 = 2.02	Fe_p = 16.5	Fe_p = 0.38
	g_2 = 2.06	Fe_d = 24.7	Fe_d = 0.63
	g_3 = 2.07		
3-$Fe_6S_6^{BS2}$	g_1 = 1.97	Fe_p = 15.5	Fe_p = 0.36
	g_2 = 2.03	Fe_d = 23.5	Fe_d = 0.60
	g_3 = 2.06		
3-$Fe_2S_2^{TRUNC}$	g_1 = 2.01	Fe_p = 22.8	Fe_p = 0.48
	g_2 = 2.05	Fe_d = 20.8	Fe_d = 0.51
	g_3 = 2.05		
3-Fe_2S_2_surr	g_1 = 2.01	Fe_p = 18.7	Fe_p = 0.44
	g_2 = 2.03	Fe_d = 21.1	Fe_d = 0.52
	g_3 = 2.04		
3-$DdH^{QM/MM}$	g_1 = 2.01	Fe_p = 15.6	Fe_p = 0.38
	g_2 = 2.05	Fe_d = 25.1	Fe_d = 0.64
	g_3 = 2.05		
Exp.	g_1 = 2.00	Fe_p = 12.4	–
	g_2 = 2.04	Fe_d = 12.4	–
	g_3 = 2.10		

Table 6. *g* factors, hyperfine couplings and Mulliken populations calculated at the BP86/TZVP level on H_{ox} models **3**. Experimental data are also included.[21]

Model name	*g* factors	Hyperfine couplings [MHz]	Mulliken spin population
3-$Fe_6S_6^{BS1}$	g_1 = 2.00	Fe_p = 12.2	Fe_p = 0.37
	g_2 = 2.03	Fe_d = 19.7	Fe_d = 0.63
	g_3 = 2.06		
3-$Fe_6S_6^{BS2}$	g_1 = 2.00	Fe_p = 10.7	Fe_p = 0.32
	g_2 = 2.02	Fe_d = 17.4	Fe_d = 0.55
	g_3 = 2.05		
3-$Fe_2S_2^{TRUNC}$	g_1 = 2.01	Fe_p = 15.9	Fe_p = 0.41
	g_2 = 2.02	Fe_d = 18.1	Fe_d = 0.59
	g_3 = 2.04		
3-Fe_2S_2_surr	g_1 = 2.01	Fe_p = 14.1	Fe_p = 0.41
	g_2 = 2.02	Fe_d = 17.6	Fe_d = 0.54
	g_3 = 2.03		
3-$DdH^{QM/MM}$	g_1 = 2.00	Fe_p = 11.9	Fe_p = 0.37
	g_2 = 2.02	Fe_d = 19.8	Fe_d = 0.62
	g_3 = 2.04		
Exp.	g_1 = 2.00	Fe_p = 12.4	–
	g_2 = 2.04	Fe_d = 12.4	–
	g_3 = 2.10		

On the other hand, the calculated Fe_p and Fe_d hyperfine couplings turned out to be closer to the experimental values, compared to those obtained for models with a vacant coordination site on Fe_d. In particular, the B3LYP hyperfine couplings are overestimated only by a factor up to 2, as shown in Table 5, while those computed at BP86 level for the water-bound adducts are even closer to the experimental results (see Table 6).

4. Corrections to the BS Solutions

In the group of Neese, the performance of the BS approach for predicting EPR parameters of tetranuclear manganese complexes has been studied.[24] It was shown that the BS approach reproduces the electron density of the system of coupled spins correctly, while the obtained spin densities and thus the EPR parameters could be incorrect. The fact that Fe_6S_6 models result in almost the same hyperfine coupling constants as Fe_2S_2 models shows that BS DFT predicts "intrinsic" hyperfine coupling constants rather than the "effective" ones.[24]

Neese and collaborators[24] have presented an approach to use BS states to calculate exchange-coupling constants. The solution of the Heisenberg exchange Hamiltonian, constructed from the obtained exchange-coupling constants, allows the calculation of on-site expectation values $<S_{zi}>$, which in turn represent correction coefficients that connect BS calculated hyperfine coupling constants with "true" estimate that could be compared with experiment. This approach has been shown to reproduce ^{55}Mn hyperfine coupling constants of the Mn_4O_xCa oxygen-evolving complex rather well. Based on this approach, the scaling factors for the $^{57}Fe/^{13}C$ hyperfine couplings of the $[2Fe]_H$ subcluster are approximately 0.51, 0.89 and 0.38 for H_{ox}-CO, H_{ox} and H_{ox}-H_2O models, respectively (using the following estimates: J_{cube} = 408, 406 and 370 cm^{-1} for H_{ox}-CO, H_{ox} and H_{ox}-H_2O models, respectively; J_H = 214, 51 and 425 cm^{-1} for the same models). These scaling factors are definitely not enough to bring calculated values for models of the **1** and **2** types to the same level of experimental data. For models of the **3** type, the use of the scaling factor would make Fe_p and Fe_d hyperfine coupling significantly lower than the experimental counterparts.

Conclusions

In the present contribution, we described a theoretical investigation of the magnetic properties of the H-cluster, using both simple Fe_2S_2 models and Fe_6S_6 models, the latter in the context of broken-symmetry calculations. The protein environment has been modelled by different approaches, viz. (i) extension of the QM region to the relevant amino acids surrounding the Fe_2S_2 subsite of the H-cluster; (ii) a continuum solvent model with ε = 40, and (iii) an all-atom representation of the enzyme in the context of hybrid QM/MM modelling. The computed *g* factors of the CO-inhibited form of the enzyme turned out to be closer to experimental findings in the case of Fe_6S_6 models of the entire H-cluster optimized by the QM/MM approach. However, it is unclear if the accurate reproduction of the effects of the

environment is actually beneficial for computation of the magnetic properties of the H-cluster at the level of theory here employed. In fact, for the H_{ox} state, the inclusion of the H-cluster surrounding in the model did not improve the computed *g* factors. Very similar conclusions can be drawn for the inclusion of the Fe_4S_4 subsite in the QM treatment: for example, for the H_{ox} state, the B3LYP results present quite large variability when one varies the BS coupling in the tetranuclear subcluster. Moreover, differences in computed *g* values are observed also when one varies the density functional (BP86 vs. B3LYP). Discrepancies in the computed *g* values were observed also in previous papers,[14,19] as a function of the level of theory and of the composition of the model; this behaviour may be related to the spin–orbit coupling, a feature that greatly complicates the calculation of EPR parameters. Notably, fluctuation of theoretical results did not impede previous authors to quite confidently characterize the redox state of the H-cluster binuclear subsite in its partially oxidized form.[19] However, such non-systematic variations prevented us to use computed *g* values in order to obtain a clear picture on the more sensitive issue of Fe_d coordination features.

More consistent results are observed in the case of hyperfine coupling calculation, which are more localised parameters and consequently their prediction is more straightforward. In this regard, we show that the accuracy of the theoretical results is rather low in absolute terms, but the ratio between Fe_p and Fe_d couplings is well reproduced for the H_{ox}-CO state.[3,6,14] Moreover, hyperfine couplings computed at BP86 level are almost independent of the extension of the QM model.

For the partially oxidized H_{ox} state, keeping in mind the above mentioned shortcomings of EPR parameters calculations, we can conclude that the theoretical *g* factors of H_{ox} models for both Fe_6S_6 and Fe_2S_2 would give a slight preference to the hypothesis of a vacant coordination site *trans* to the bridging CO on Fe_d. However, the hyperfine coupling constants and thus the distribution of the spin density in the binuclear subcluster are much closer to the experimental data when a water ligand is coordinated to the Fe_d atom. Therefore, even if on the basis of the present data we cannot conclusively reject any of these two models, the model of the H_{ox} state featuring a coordinated water ligand (H_{ox}-H_2O) is slightly preferable. Indeed, previous QM/MM results have highlighted that weak coordination of a water molecule to the Fe_d atom is possible if the chelating ligand bridging the two iron atoms of the binuclear subcluster is dithiomethylamine (DTMA), due to the formation of a hydrogen bond between the amine group of DTMA and the water oxygen atom.[25]

Methodological Section

Geometry optimizations of purely QM Fe_6S_6 models (**1-$Fe_6S_6^{BS1}$**, **1-$Fe_6S_6^{BS2}$**, **2-$Fe_6S_6^{BS1}$**, **2-$Fe_6S_6^{BS2}$**, **3-$Fe_6S_6^{BS1}$**, **3-$Fe_6S_6^{BS2}$**) were carried out using TURBOMOLE program suite,[26] at the BP86/TZVP level,[27] and making use of the resolution of identity (RI) technique;[28] the energy difference values reported in this paper were computed at such level of theory. In the optimization of the Fe_6S_6 models, all the cysteine alpha carbon atoms were constrained at their crystallographyc position,[1] and the COSMO continuum solvent model[16] was used, with a dielectric constant $\varepsilon = 40$; such a dielectric constant value turned out to best reproduce the CO-bridged geometry expected for the H_{ox} form of the enzyme, based on crystallographic data.[1–3] From these optimized geometries, truncated models of the H-cluster were also obtained (**1-$Fe_2S_2^{TRUNC}$**, **2-$Fe_2S_2^{TRUNC}$**, **3-$Fe_2S_2^{TRUNC}$**), by substituting their $[Fe_4S_4](SCH_3)_3$ fragment with a hydrogen atom. In all cases, this hydrogen atom was bonded to the cysteine sulfur atom belonging to Fe_p coordination sphere. The resulting SH bond was assigned a 1.3 Å distance in all models.

At the next level of approximation, models of nine amino acids surrounding the Fe_2S_2 cluster were included (see Figure S1 in the Supporting Information). The atomic composition and initial geometry of these models were obtained as described previously.[17] These models underwent constrained geometry optimizations in the COSMO continuum solvent at $\varepsilon = 40$. The constrained atoms are specified in the Supporting information (Figure S1).

As for the optimization of the QM/MM models, the COMQUM program was used,[29] and the apporach already described by us was applied,[25] with the only difference that all calculations have been carried out using the large TZVP basis, in place of the smaller SVP basis used in our previous study. More generally, all the SCF calculation performed along the geometry optimizations here described were carried out at BP86-RI/TZVP level, using the broken-symmetry approach[23] in the case of Fe_6S_6 models (see Supporting Information for details on spin distributions in the BS1 and BS2 wavefunctions, Figure S3. These two electronic states present opposite spin localization patterns on the Fe_4S_4 subcluster, while the α-spin excess on the binuclear subcluster is always left unaltered. Thus, both the possible cases of ferromagnetic and antiferromagnetic coupling between the Fe_2S_2 subsite and the closest Fe atom in the Fe_4S_4 moiety are taken into account here). To obtain broken-symmetry wavefunctions featuring specific patterns of spin excess on the H-cluster tetranuclear subsite, we applied an approach recently described by us.[30]

DFT calculations of *g* factors and hyperfine couplings was carried out using the ORCA 2.6 program,[31] both at the BP86-RI/TZVP and the B3LYP/TZVP level.[32] The TPSS and TPSSh functionals,[33] successfully used for hyperfine couplings computation in previous studies,[34] were also tested on models **1-$Fe_2S_2^{TRUNC}$**, **2-$Fe_2S_2^{TRUNC}$**, **3-$Fe_2S_2^{TRUNC}$**; the resulting overall picture turned out to be very similar to that obtained at BP86 and B3LYP level (data not shown).

Supporting Information (see footnote on the first page of this article): Graphical representation of the composition of QM models including relevant portions of the protein matrix; optimized structures of models featuring a water molecule coordinated to Fe_d; graphical representation of the spin excess pattern in the BS solutions considered in the study.

Acknowledgments

C. G. acknowledges support from the Humboldt Foundation.

[1] Y. Nicolet, C. Piras, P. Legrand, C. E. Hatchikian, J. C. Fontecilla-Camps, *Struct. Folding Des.* **1999**, *7*, 13–23.
[2] J. W. Peters, W. N. Lanzilotta, B. J. Lemon, L. C. Seefeldt, *Science* **1998**, *282*, 1853–1858; A. S. Pandey, T. V. Harris, L. J.

Giles, J. W. Peters, R. K. Szilagyi, *J. Am. Chem. Soc.* **2008**, *130*, 4533–4540.

[3] B. J. Lemon, J. W. Peters, *Biochemistry* **1999**, *38*, 12969–12973.

[4] Y. Nicolet, A. L. de Lacey, X. Vernede, V. M. Fernandez, E. C. Hatchikian, J. C. Fontecilla-Camps, *J. Am. Chem. Soc.* **2001**, *123*, 1596–1601.

[5] W. Roseboom, A. L. De Lacey, V. M. Fernandez, E. C. Hatchikian, S. P. J. Albracht, *J. Biol. Inorg. Chem.* **2006**, *11*, 102–118.

[6] Z. J. Chen, B. J. Lemon, S. Huang, D. J. Swartz, J. W. Peters, K. A. Bagley, *Biochemistry* **2002**, *41*, 2036–2043.

[7] A. Silakov, C. Kamp, E. Reijerse, T. Happe, W. Lubitz, *Biochemistry* **2009**, *48*, 7780–7786.

[8] Z. X. Cao, M. B. Hall, *J. Am. Chem. Soc.* **2001**, *123*, 3734–3742.

[9] W. Lubitz, E. Reijerse, M. van Gastel, *Chem. Rev.* **2007**, *107*, 4331–4365.

[10] A. S. Pereira, P. Tavares, I. Moura, J. J. G. Moura, B. H. Huynh, *J. Am. Chem. Soc.* **2001**, *123*, 2771–2782; C. V. Popescu, E. Munck, *J. Am. Chem. Soc.* **1999**, *121*, 7877–7884.

[11] M. Bruschi, C. Greco, G. Zampella, U. Ryde, C. J. Pickett, L. De Gioia, *C. R. Chim.* **2008**, *11*, 834–841; H. J. Fan, M. B. Hall, *J. Am. Chem. Soc.* **2001**, *123*, 3828–3829.

[12] P. E. M. Siegbahn, J. W. Tye, M. B. Hall, *Chem. Rev.* **2007**, *107*, 4414–4435.

[13] S. P. J. Albracht, W. Roseboom, E. C. Hatchikian, *J. Biol. Inorg. Chem.* **2006**, *11*, 88–101.

[14] C. Greco, M. Bruschi, J. Heimdal, P. Fantucci, L. De Gioia, U. Ryde, *Inorg. Chem.* **2007**, *46*, 7256–7258.

[15] M. Bruschi, C. Greco, P. Fantucci, L. De Gioia, *Inorg. Chem.* **2008**, *47*, 6056–6071.

[16] A. Klamt, *J. Phys. Chem.* **1995**, *99*, 2224–2235.

[17] A. Silakov, B. Wenk, E. Reijerse, W. Lubitz, *Phys. Chem. Chem. Phys.* **2009**, *11*, 6592–6599.

[18] A. Silakov, B. Wenk, E. Reijerse, S. P. J. Albracht, W. Lubitz, *J. Biol. Inorg. Chem.* **2009**, *14*, 301–313.

[19] A. T. Fiedler, T. C. Brunold, *Inorg. Chem.* **2005**, *44*, 9322–9334.

[20] M. van Gastel, C. Fichtner, F. Neese, W. Lubitz, *Biochem. Soc. Trans.* **2005**, *33*, 7–11.

[21] A. Silakov, E. J. Reijerse, S. P. J. Albracht, E. C. Hatchikian, W. Lubitz, *J. Am. Chem. Soc.* **2007**, *129*, 11447–11458.

[22] D. E. Schwab, C. Tard, E. Brecht, J. W. Peters, C. J. Pickett, R. K. Szilagyi, *Chem. Commun.* **2006**, 3696–3698.

[23] L. Noodleman, J. G. Norman, *J. Chem. Phys.* **1979**, *70*, 4903–4906; L. Noodleman, *J. Chem. Phys.* **1981**, *74*, 5737–5743.

[24] D. A. Pantazis, M. Orio, T. Petrenko, S. Zein, E. Bill, W. Lubitz, J. Messinger, F. Neese, *Chem. Eur. J.* **2009**, *15*, 5108–5123.

[25] C. Greco, M. Bruschi, L. De Gioia, U. Ryde, *Inorg. Chem.* **2007**, *46*, 5911–5921.

[26] R. Ahlrichs, M. Bar, M. Haser, H. Horn, C. Kolmel, *Chem. Phys. Lett.* **1989**, *162*, 165–169.

[27] A. D. Becke, *Phys. Rev. A* **1988**, *38*, 3098–3100; J. P. Perdew, *Phys. Rev. B* **1986**, *33*, 8822–8824; A. Schafer, C. Huber, R. Ahlrichs, *J. Chem. Phys.* **1994**, *100*, 5829–5835.

[28] K. Eichkorn, O. Treutler, H. Ohm, M. Haser, R. Ahlrichs, *Chem. Phys. Lett.* **1995**, *240*, 283–289; K. Eichkorn, F. Weigend, O. Treutler, R. Ahlrichs, *Theor. Chem. Acc.* **1997**, *97*, 119–124.

[29] U. Ryde, *J. Computer-Aided Mol. Des.* **1996**, *10*, 153–164; U. Ryde, M. H. M. Olsson, *Int. J. Quantum Chem.* **2001**, *81*, 335–347.

[30] C. Greco, P. Fantucci, U. Ryde, L. De Gioia, *International Journal of Quantum Chemistry*, in press; DOI: 10.1002/qua.22849.

[31] F. Neese, *ORCA – An* ab initio, *Density Functional and Semiempirical Program Package*, University of Bonn, Bonn, Germany, **2007**.

[32] A. D. Becke, *J. Chem. Phys.* **1993**, *98*, 5648–5652; C. T. Lee, W. T. Yang, R. G. Parr, *Phys. Rev. B* **1988**, *37*, 785–789.

[33] J. P. Perdew, J. M. Tao, V. N. Staroverov, G. E. Scuseria, *J. Chem. Phys.* **2004**, *120*, 6898–6911; V. N. Staroverov, G. E. Scuseria, J. M. Tao, J. P. Perdew, *J. Chem. Phys.* **2003**, *119*, 12129–12137; J. M. Tao, J. P. Perdew, V. N. Staroverov, G. E. Scuseria, *Phys. Rev. Lett.* **2003**, *91*; V. N. Staroverov, G. E. Scuseria, J. Tao, J. P. Perdew, *Phys. Rev. B* **2004**, *69*, 11.

[34] S. Kossmann, B. Kirchner, F. Neese, *Mol. Phys.* **2007**, *105*, 2049–2071; M. Orio, D. A. Pantazis, F. Neese, *Photosynthesis. Res.* **2009**, *102*, 443–453.

Received: October 4, 2010
Published Online: January 20, 2011

